analytical chemistry

pubs.acs.org/ac Article

Electrochemical Aptamer Biosensor Based on ATP-Induced 2D DNA Structure Switching for Rapid and Ultrasensitive Detection of ATP

Ying Liu, Lingqi Kong, Hao Li, Ruo Yuan,* and Yaqin Chai*

Cite This: *Anal. Chem.* 2022, 94, 6819−6826 Read Online

ACCESS | Metrics & More | Article Recommendations | Supporting Information

ABSTRACT: Herein, a two-dimensional (2D) DNA structure with multiple ATP aptamers was elegantly designed to establish an electrochemical biosensor for rapid and sensitive detection of ATP based on ATP-induced structure switching. Concretely, the prepared 2D DNA structure containing numerous ATP aptamers as ATP-specific toehold switches could not only immobilize a large number of methylene blue (MB) for generating a remarkable electrochemical signal, but also greatly increase the local concentration of ATP aptamers to obviously enhance the capture efficiency of ATP. Once the target ATP interacted with the toehold switches, the 2D DNA structure could be sharply collapsed to trigger the burst release of MB from the electrode surface, ultimately resulting in a significantly decreased electrochemical signal for ultrasensitive detection of target ATP over a short period of time. Impressively, by dexterously adjusting the length of the ATP-specific toehold switches to 15-base, optimization of the binding affinity between ATP and the toehold switches was achieved for cutting down the detection time to 30 min and achieving a low detection limit of 0.3 pM, which addressed the shortcoming of time-consuming and poor sensitivity in the previous sensors with a small quantity of ATP aptamers and deficient binding affinity to ATP. Consequently, this strategy opened a promising avenue for ultrasensitive and rapid detection of various biomolecules in biomedical application and disease diagnosis.

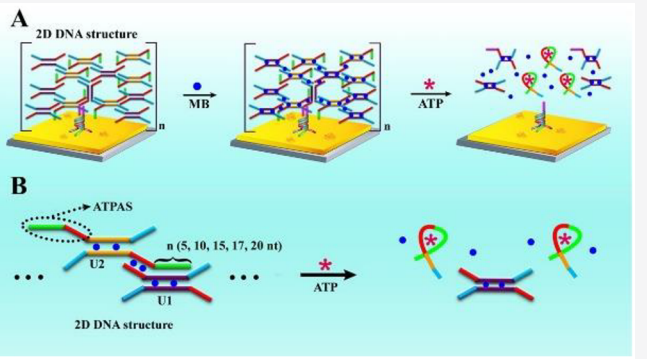

Downloaded via SEOUL NATL UNIV on November 6, 2022 at 10:58:44 (UTC).
See https://pubs.acs.org/sharingguidelines for options on how to legitimately share published articles.

INTRODUCTION

Adenosine triphosphate (ATP) as the energy currency is an essential small biological molecule in living organisms,[1−5] which plays an important role in regulating cell metabolism, participating in all kinds of enzyme reactions and guiding the life activities of tissues and cells.[6,7] An abnormal level of ATP has been demonstrated to be relevant to many diseases, such as Parkinson's disease, Alzheimer's disease, and angiocardiopathy.[8−11] Hence, it is of great significance for human health to establish rapid, sensitive, and specific analytical methods for ATP detection. Nowadays, the aptamer-based methods have attracted wide and increasing attention due to the advantages of aptamer, like their small size, high stability, easy synthesis, high designability, and low cost.[12−17] The biosensors coupled with aptamer strategies have been employed to specifically detect ATP based on the distinctive binding affinity between ATP and the aptamer.[18−28] However, the traditional aptamer biosensors always suffered from slow detection speed and low sensitivity tissues due to the deficient binding affinity of ATP and weak capture efficiency of ATP, as well as low loading capacity of molecular beacons. Therefore, it is urgently required to develop a new type of DNA structure that could not only significantly improve the capture efficiency and binding affinity of the target ATP, but also enhance the loading capacity of the signal molecule for the great promotion of detection speed and sensitivity. In this work, a two-dimensional (2D) DNA structure with a large number of ATP aptamers as ATP-specific toehold switches was proposed to construct an ultrasensitive electrochemical biosensor based on ATP-induced structure switching, which could immobilize a mass of signal molecules and demonstrate significant enhancement of the capture efficiency of the target ATP for realizing rapid and sensitive ATP detection. Impressively, by engineering the length of the toehold switches, the optimal binding affinity between ATP and toehold switches was obtained to further vastly accelerate the detection speed and greatly improved the detection sensitivity.

Herein, the electrochemical aptamer-based biosensor combined with a novel 2D DNA structure with multiple ATP aptamers was developed to sensitively detect target ATP with high speed via ATP-induced structure switching. The specific construction processes were illustrated in Scheme 1A,

Received: February 6, 2022
Accepted: April 13, 2022
Published: April 26, 2022

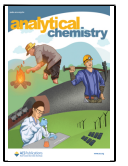

ACS Publications © 2022 American Chemical Society

https://doi.org/10.1021/acs.analchem.2c00613
Anal. Chem. 2022, 94, 6819−6826

Scheme 1. Schematic Illustration of (A) the Proposed Electrochemical Aptamer Biosensor Based on ATP-Induced 2D DNA Structure Switching for Rapid and Ultrasensitive Detection of ATP; (B) Regulation of the Length of Toehold for Rapid Release of MB

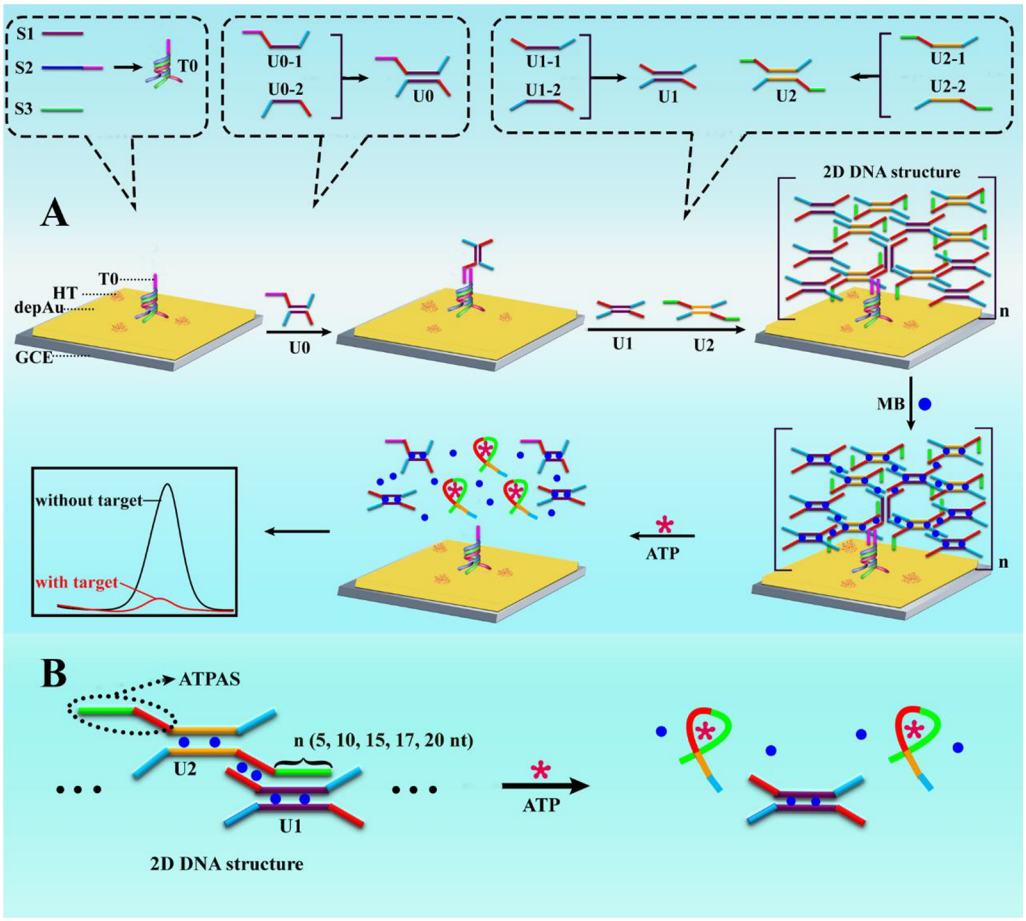

with the triple-stranded DNA (T0) bearing three polyadenine (poly(A)) tails as a rigid scaffold was first immobilized on the electrode through the strong affinity interaction between the poly(A) tails and the gold nanoparticle, and then the double-stranded DNA (U0) was efficiently captured on the sensing platform by complementing to the overhand DNA strand (the purple fragment) of T0. Subsequently, the 2D DNA structure was formed by the self-assembly of two double-stranded DNA (U1 and U2) on the basis of the complementary nucleotide matching. After that, the 2D DNA structure with an abundant DNA double helix was assembled on the modified electrode by hybridizing with U0 to immobilize numerous MB for yielding a remarkable electrochemical signal. In particular, U2 was designed with an ATP aptamer sequence (ATPAS) at both ends, in which a part of the ATPAS (the red fragment) was used to hybridize with U1 to form the 2D DNA structure and the other part of the ATPAS (the green fragment) was exposed as ATP-specific toehold switches to react with ATP. In this ingenious design, massive ATP-specific toehold switches were embedded into the 2D DNA structure to greatly enhance the capture efficiency between ATP and the aptamer. While the target ATP was dropped onto the established sensing platform, the 2D DNA structure would be dissociated, owing to the ultrahigh affinity between ATP and the toehold switches to rapidly release a lot of MB and thereby lead to a dramatically reduced electrochemical signal for ultrasensitive detection of ATP in a short time. Impressively, by adjusting the length of the exposed toehold in toehold switches to 15-base (Scheme 1B), the optimal binding affinity between ATP and the aptamer was obtained, which could further promote ultrasensitive detection of ATP in just 30 min. In short, the proposed sensing strategy provided an attractive method to design the high-performance biosensor for rapid and sensitive detection of various biomarkers, which paved a promising avenue in disease diagnosis and bioanalysis.

EXPERIMENTAL SECTION

Preparation of Triple-Stranded DNA. First, an equimolar concentration (4 μM) of three single-stranded DNA, S1, S2, and S3, was mixed in TNM buffer (see Supporting Information). After that, the mixture solution was used to react for 2 h at 37 °C to form a triple-stranded DNA (T0), and the resulting T0 was stored at 4 °C for later use.

Synthesis of Two-Dimensional DNA Structure. The double-stranded DNA1 (U1) was fabricated by self-assembling single-stranded DNA U1−1 and U1−2 (1:1 molar ratio) in 2× SSC buffer for 2 h at 37 °C. Similarly, the double-stranded DNA2 (U2) was formed by single-stranded DNA U2−1 and U2−2 with a complementary nucleotide matching their intermediate sequence, which both are labeled with an ATP aptamer sequence at the 5′-terminal. The concentration of products U1 and U2 was 2 μM, and then the two-dimensional (2D) DNA structure was assembled by mixing the prepared U1 and U2 at a molar ratio of 1:6 at 37 °C for 1.5 h.

https://doi.org/10.1021/acs.analchem.2c00613
Anal. Chem. 2022, 94, 6819−6826

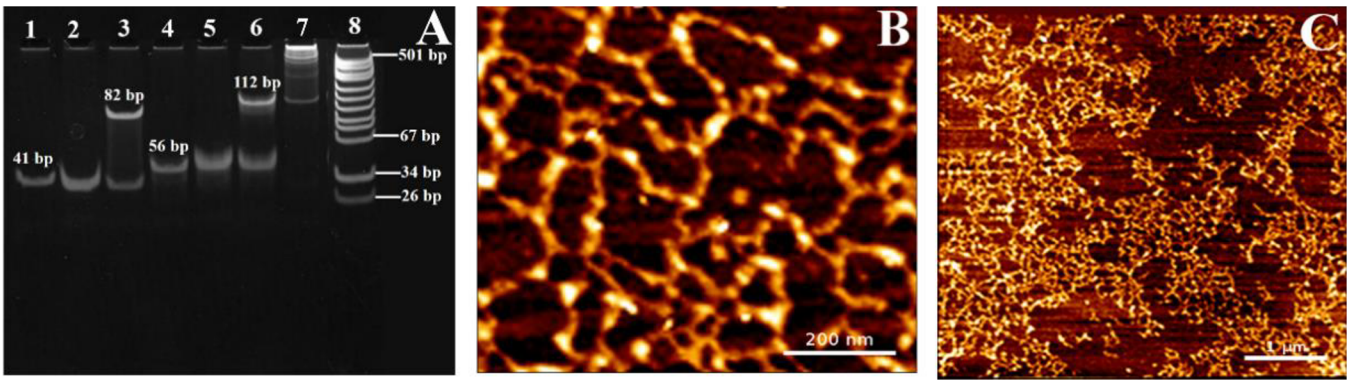

Figure 1. (A) Evaluation of the 2D DNA structure using gel electrophoresis, lane 1, U1−1; lane 2, U1−2; lane 3, U1; lane 4, U2−1; lane 5, U2−2; lane 6, U2; lane 7 is the hybridized product of U1 and U2; lane 8 is the DNA marker. (B, C) AFM characterization of the 2D DNA structure.

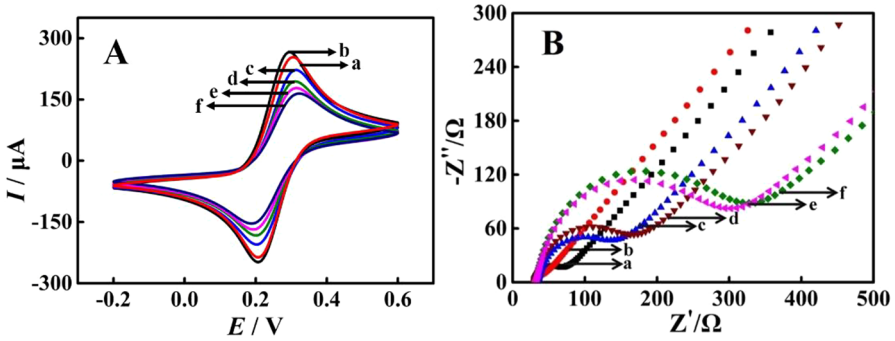

Figure 2. (A) CV and (B) EIS characterizations of the modified electrode: (a) bare GCE, (b) depAu/GCE, (c) T0/depAu/GCE, (d) HT/T0/depAu/GCE, (e) U0/HT/T0/depAu/GCE, and (f) 2D DNA structure/U0/HT/T0/depAu/GCE.

Fabrication of the Biosensor for Detecting Adenosine Triphosphate. Prior to the immobilization of T0, the bare glassy carbon electrode (GCE) was polished with alumina slurries to obtain a clean bare GCE. Subsequently, the cleaned GCE was electrodeposited in $HAuCl_4$ solution (1%) for 30 s at 0.2 V to obtain the gold particles (depAu). Subsequently, 10 μL of the as-prepared T0 was added onto the electrode for incubating overnight at 4 °C. Then, 10 μL of 1 mM 1-hexanethiol (HT) was immobilized on the modified electrode surface at room temperature for 20 min to block the nonspecific sites. Afterward, double-stranded DNA0 (U0; 2 μM) was synthesized by mixing U0−1 and U0−2 (1:1 molar ratio) in 2× SSC buffer at 37 °C for 2 h, and then 10 μL of U0 and 10 μL of 2D DNA structure were dropped into the above electrode surface for 2 h at 37 °C, separately. Thereafter, 10 μL of 20 μM methylene blue (MB) were added in the electrode surface at 37 °C for 30 min. Next, the electrode was cleaned by ultrapure water in each step, and the finished electrode as the biosensor was used to detect target adenosine triphosphate (ATP).

RESULTS AND DISCUSSION

Characterization of the Two-Dimensional DNA Structure. In this work, the successful formation of the 2D DNA structure was demonstrated by the native polyacrylamide gel electrophoresis (PAGE). As depicted in Figure 1A, lanes 1 and 2 are U1−1 and U1−2, respectively. The hybridization product of U1−1 and U1−2 was matched in lane 3, which had a larger molecular weight with slow mobility. Similarly, lanes 4 and 5 represent U2−1 and U2−2, respectively. Lane 6 is the hybridized product of U2−1 and U2−2. Furthermore, lane 7 corresponds to the hybridized product of U1 and U2. The bright band with extremely lower mobility could be clearly observed in lane 7, which demonstrated the successful generation of a 2D DNA structure with a large molecular weight. Additionally, lane 8 is the DNA marker. In addition, the atomic force microscopy (AFM; Figure 1B,C) was implemented to demonstrate the formation of the 2D DNA structure. To sum up, these results demonstrated the 2D DNA structure was generated successfully.

Electrochemical Characterization of the Electrode Modification. Cyclic voltammetric (CV) and electrochemical impedance spectroscopy (EIS) was used to characterize the proposed biosensor for ATP detection in 5 mM $[Fe(CN)_6]^{3-/4-}$ solution. The scanning potential of CV was from −0.2 to 0.6 V. First, as seen in the Figure 2A, an obvious redox peak (curve a) of the bare GCE could be discovered. Then a higher redox peak (curve b) of the depAu-modified electrode would be observed, which could be explained that depAu could promote the electron-transfer process. As T0 and blocking agent HT were gradually introduced into the electrode, the redox peaks (curves c and d) decreased step by step. Because of the electrostatic expelling effect between the negatively charged phosphate backbone of the DNA and $[Fe(CN)_6]^{3-/4-}$, the peak current (curve e) further decreased with the incubation of U0. Certainly, the peak current (curve f) would decline when the 2D DNA structure was immobilized on the electrode due to the high hindrance of negatively charged 2D DNA structure.

Meanwhile, from Figure 2B, EIS was also utilized to characterize the modified electrode. The value of the electron-transfer resistance (R_{et}) of depAu/GCE (curve b)

https://doi.org/10.1021/acs.analchem.2c00613
Anal. Chem. 2022, 94, 6819−6826

was smaller than the bare GCE (curve a), which could be simply explained using the excellent conductivity of depAu. Successively, the R_{et} value increased gradually with the attachment of negatively charged T0 (curve c) and non-conductive HT (curve d) in succession. Thereafter, the impedance values of U0/HT/T0/depAu/GCE and 2D DNA structure/U0/HT/T0/depAu/GCE would keep increasing undoubtedly, due to the repulsive electrostatic effect. The above CV results were consistent with EIS data, which indicated the successful stepwise fabrication of the proposed biosensor.

Feasibility of the Biosensor for Detecting ATP. In addition, square wave voltammetry (SWV) was employed to explore the feasibility of the electrochemical biosensor. Figure 3C depicts the significant SWV signal of MB without target

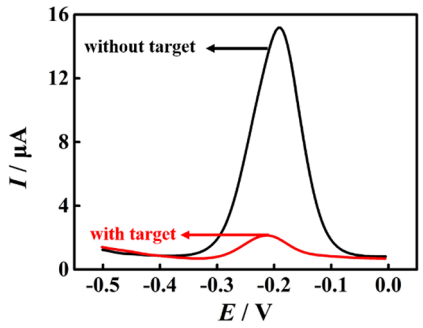

Figure 3. SWV responses of without ATP and with ATP (10 nM). The signals were obtained in 0.1 M PBS solution (pH 7.0).

ATP, suggesting that a large number of MB molecules intercalated in the 2D DNA structure with abundant double helix structures. Inversely, the current greatly decreased in the presence of target ATP, which illustrated that the ATP-specific DNA toehold switches designed in the 2D DNA structure would strongly bind to target ATP to disrupt the hybridized DNA helix, finally leading to the dissociation of the 2D DNA structure to release a lot of MB molecules. The above conclusions proved that the proposed strategy exhibited excellent potential applications for ATP detection.

Optimization of the Experimental Conditions. Lots of factors influence the performance of the electrochemical biosensor, so investigating the optimum experimental conditions is indispensable. First, because the forming efficiency of the 2D DNA structure was closely linked to U1 and U2, the stoichiometry ratio between U1 and U2 was optimized. As seen in Figure 4A, as the proportion of U1 and U2 changed from 1:1 to 1:10, the SWV response increased gradually and reached a platform at 1:6. Thus, the stoichiometry ratio of 1:6 was eventually identified as the optimum ratio of U1 and U2. Moreover, pH would affect the stability of the triplex generation to further impact the electrochemical response, owing to the well-characterized pH sensitivity of triplex DNA. Accordingly, the pH of T0 formation was studied and the results received from Figure 4B show that the current increased gradually as the value of pH grew from 5 to 6. However, with the further increasing value of pH, the triplex was separated to ultimately generate a decline of the current values. Therefore, pH 6 was employed as the optimum pH for the following experiments. Additionally, the concentration of Mg^{2+} acting as an important role to produce the 2D DNA structure was investigated. As depicted in Figure 4C, the current increased continually, with the Mg^{2+} concentration ranging from 5 to 15 mM and having a tendency to decrease after 15 mM. Thus, 15 mM was selected as the optimal concentration of Mg^{2+}. Furthermore, the hybridization time of the U1 and U2 had a great impact on the efficiency and stability of the 2D DNA structure. Thus, the hybridization time of U1 and U2 was investigated. According to Figure 4D, the current increased continually with the increment of hybridization time and reached a plateau at 1.5. Therefore, the optimal hybridization time of the 2D DNA structure was 1.5 h. In principle, the electrochemical signal came from MB, thus effects of the concentration of MB on the SWV response signal of the proposed biosensor were investigated. As illustrated in Figure 4E, the current increased gradually, with the MB concentration increasing from 5 to 20 μM and reaching a plateau at 20 μM. Therefore, the 20 μM as the optimal concentration of MB was utilized in this work. All the current signals were obtained by SWV in PBS solution (pH 7.0) with a 10 nM target ATP.

Regulation of the Binding Affinity between ATP and Different Lengths of Toehold. To obtain the optimal binding affinity between ATP and the exposed toehold for rapid release of MB, the length of the toehold was regulated by changing the length of the sequences at both ends of U1, which was complementary to the ATP aptamer sequences (ATPAS). From Figure 5, with the increasing length of toehold, the release rate of MB increased gradually due to the fact that a longer toehold displayed a stronger binding affinity of ATP, and when the exposed toehold was up to 15-base, the release of MB finished in 30 min. Additionally, with the further increasing length of exposed toehold, less bases in ATPAS could hybridize with U1, resulting in the instability of the synthesized 2D DNA structure to ultimately generate false positive results. In summary, a 15-base toehold was employed to obtain the optimal binding affinity for promoting rapid and ultrasensitive detection of ATP.

Analytical Performance of the Proposed Biosensor. To analyze the performance of the proposed biosensor, various concentrations of target ATP were detected by the proposed biosensor under optimal conditions. As shown in Figure 6A, the SWV response currents were gradually decreased with the concentration of ATP increased from 1pM to 100 μM. Besides, Figure 6B showed the correlation between the current and the logarithm (lg) of ATP concentration, the regression equation was $I = 4.340-0.3830 \lg c_{target}$ ($r = -0.9972$) and the limit of detection (LOD) was 0.3 pM. Specifically, compared with the other methods, the proposed work exhibited a wider linear range and lower detection limit (Table 1) on account of the effective formation of the 2D DNA structure, which possessed numerous ATP aptamers to significantly enhance the capture efficiency of ATP. Consequently, the proposed biosensor indicated superior sensitivity and excellent performance in ATP detection.

Selectivity, Reproducibility, and Stability of the Biosensor. To confirm the specificity of the biosensor, we chose glutathione (GSH), bovine serum albumin (BSA), α-1-fetoprotein (AFP), and thrombin (TB) as interfering agents (each at 1000 nM). As shown in Figure 7A, the interfering agents were used to investigate, and nearly identical current values were observed. On the contrary, a small concentration of ATP (10 nM) was introduced into the sensing platform to cause a significant current value decrease. Moreover, the mixture sample containing ATP (10 nM) and all interference proteins (each at 1000 nM) resulted in a low current value. As

https://doi.org/10.1021/acs.analchem.2c00613
Anal. Chem. 2022, 94, 6819−6826

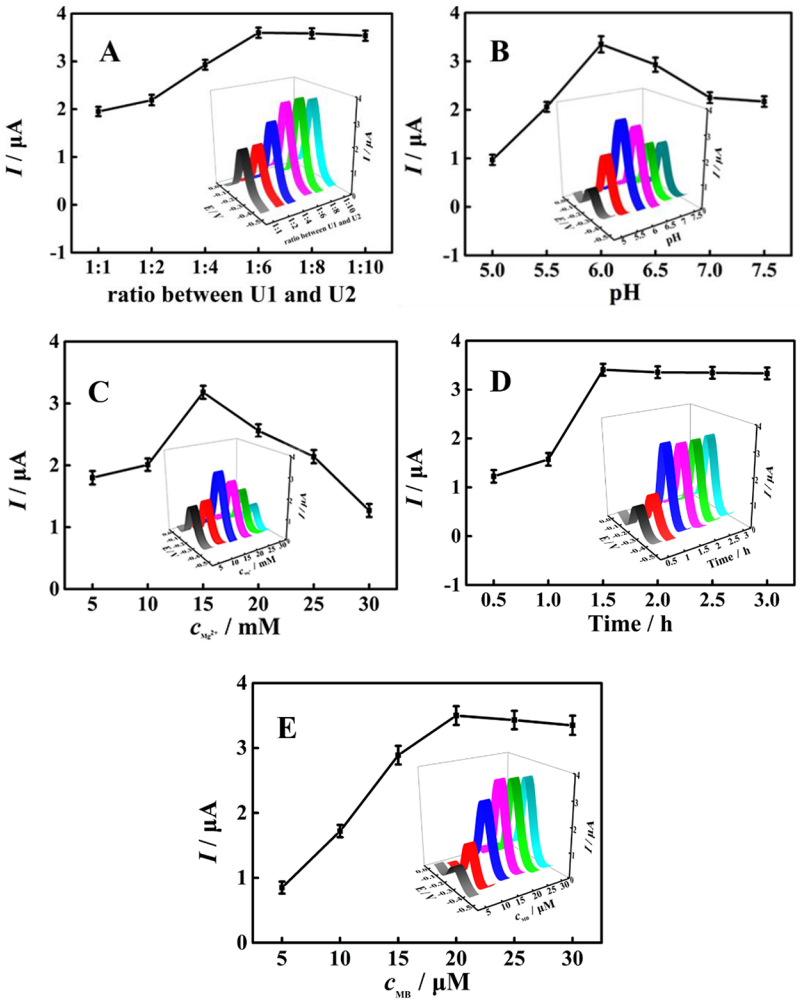

Figure 4. (A) Effect of ratio between U1 and U2 on electrode responses. (B) pH optimization of T0 formation. (C) SWV response of the proposed biosensor at different concentration of Mg^{2+}. (D) Optimization of the hybridization time between U1 and U2 for generation of 2D DNA structure. (E) Optimum of the concentration of MB. The SWV responses of the proposed sensor were obtained in 0.1 M PBS (pH 7.0). Error bars: standard deviation (SD), n = 3.

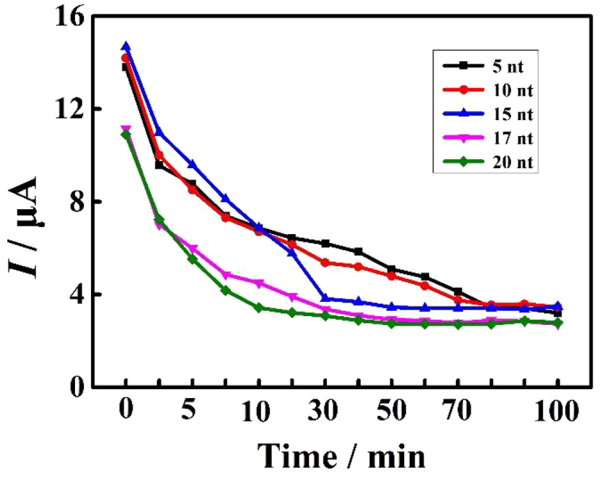

Figure 5. MB release profile of the 2D DNA structure with different lengths of toehold. Error bars: standard deviation (SD), n = 3.

a whole, it indicated good selectivity of the biosensor toward ATP. Significantly, an acceptable reproducibility of the biosensor was necessary (Figure 7B). Therefore, reproducibility was explored with different batches of developed biosensors to detect 10 nM ATP, with the response values of the biosensors being similar and RSD was 4.1%. These figures suggested that the present biosensor held significant reproducibility. Stability played a significant role in biosensor performance and was tested under optimized conditions (Figure 7C). Next, the current value was measured every 4 days, and it was found that the current value could still be maintained at 91.04% of the initial value after 16 days, which illustrated that the posed sensing platform possessed excellent stability. In addition, the biosensor was constructed to detect the 50-fold diluted healthy serum samples spiked with 10 nM ATP. Then, the current value was measured every 4 days, and as Figure 7D showed, with the increase of the storage time, the current intensity was approximately consistent, suggesting that the proposed biosensor was stable for serum samples.

Application of the Biosensor for Serum Samples and Artificial Cerebrospinal Fluid (aCSF) Sample Detection. In order to explore the feasibility of the proposed electrochemical biosensor for real samples, we designed the recovery experiments. At first, the 50-fold diluted healthy serum samples and aCSF (see Supporting Information) spiked with different concentrations of the target ATP (0.1, 1, 10, and 100 nM) were tested impressively, acquiring a gratifying recoveries range

https://doi.org/10.1021/acs.analchem.2c00613
Anal. Chem. 2022, 94, 6819−6826

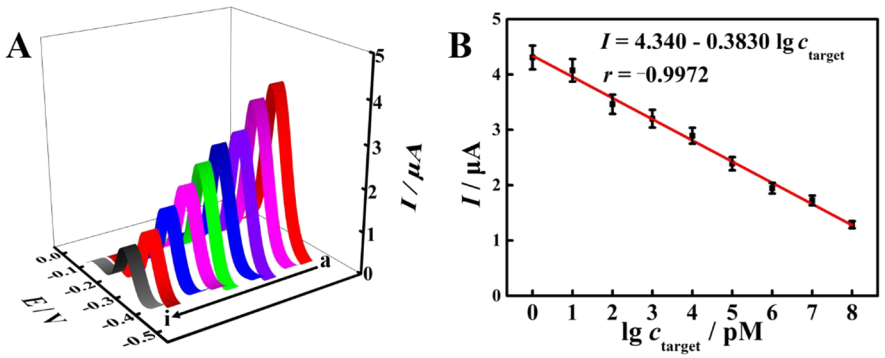

Figure 6. (A) SWV responses of the proposed biosensor in the presence of various concentrations of ATP (from curve a to curve i): 1 pM, 10 pM, 100 pM, 1 nM, 10 nM, 100 nM, 1 μM, 10 μM, and 100 μM. (B) The calibration plot of SWV response currents vs the logarithm of target concentrations. Error bars: standard deviation (SD), n = 3.

Table 1. Comparison of Proposed Biosensor with Other Reported Works for ATP Detection

analytical method	linear range	detection limit	ref
colorimetric	10 nM to 18 μM	8.4 nM	29
fluorescent	\	17 nM	30
fluorescent	10 μM to 0.3 mM	0.3 μM	31
fluorescent	100−2 mM	18 μM	32
electrochemical	1−100 μM	1 μM	33
electrochemical	50 μM to 2 mM	26 μM	34
electrochemical	1 pM to 100 μM	0.3 pM	this work

from 97.04% to 108.1%, with satisfactory RSD in the range of 2.8% to 4.2%, illustrated in Table 2. Table 3 lists the acceptable recoveries as from 97.04% to 101.8%, with a RSD between 3.1% and 4.6%, which confirmed the potential application of the biosensor in complex biological samples.

Table 2. Recovery Results of ATP Added in Human Serums (n = 3)

sample number	added (nM)	found (nM)	recovery (%)	RSD (%)
1	0.1	0.1006	100.6	4.2
2	1	1.024	102.4	3.6
3	10	10.81	108.1	3.9
4	100	97.04	97.04	2.8

Table 3. Detection of ATP Added in aCSF (n = 3)

sample number	added (nM)	found (nM)	recovery (%)	RSD (%)
1	0.1	0.1018	101.8	3.3
2	1	0.9704	97.04	4.6
3	10	10.09	100.9	3.4
4	100	98.21	98.21	3.1

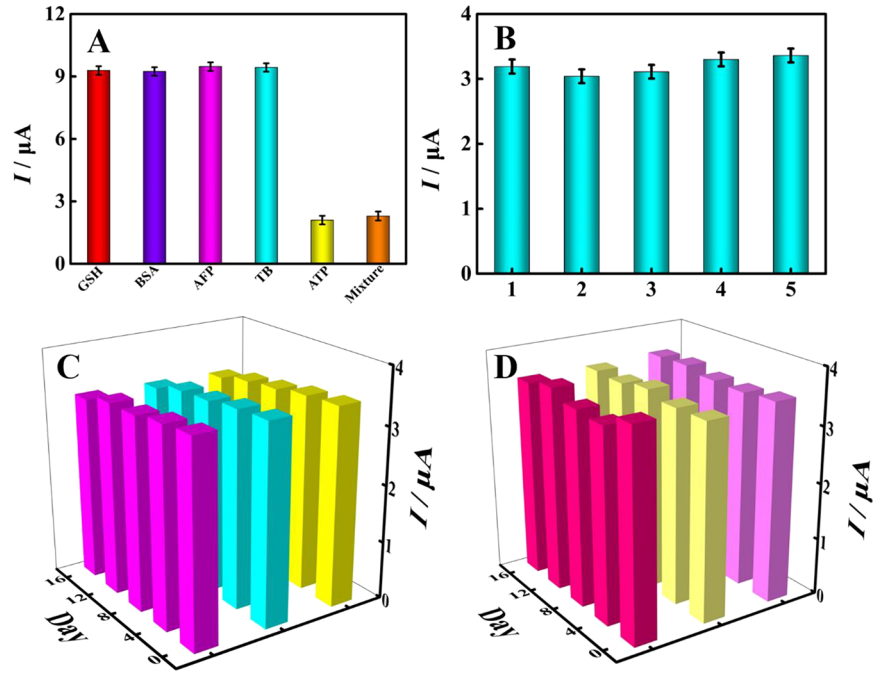

Figure 7. (A) Selectivity of the proposed biosensor for ATP (10 nM) against other interferences. (B) Reproducibility of the proposed sensing platform. (C) Study of stability performances. (D) Stability of the proposed biosensor for ATP detection in serum samples. Error bars: standard deviation (SD), n = 3.

https://doi.org/10.1021/acs.analchem.2c00613
Anal. Chem. 2022, 94, 6819−6826

CONCLUSIONS

In conclusion, a novel electrochemical biosensor with developed by integrating the 2D DNA structure with an abundance of ATP aptamers as ATP-specific toehold switches were successfully fabricated for rapid and ultrasensitive detection of ATP with the use of the strategy of ATP-induced structure switching. Surprisingly, this study showed distinctive advantages as follows: First, a large quantity of MB as electrochemical signal molecules could be allowed to intercalate into the employment of the 2D DNA structure for obtaining a significant electrochemical signal. Second, the proposed 2D DNA structure combined multiple ATP aptamers as ATP-specific toehold switches to greatly enhance the capture efficiency between ATP and the aptamer, ultimately resulting in rapid and ultrasensitive detection of ATP. Finally, the detection sensitivity and speed could be further improved by tuning the length of the ATP-specific toehold switches for optimal binding affinity between ATP and toehold switches. To sum up, the proposed biosensor platform showed excellent performance for rapid and ultrasensitive analysis of various biomarkers, which paved the prospective way for application in clinical diagnoses.

ASSOCIATED CONTENT

Supporting Information

The Supporting Information is available free of charge at https://pubs.acs.org/doi/10.1021/acs.analchem.2c00613.

Materials and reagents, apparatus, comparison study of different biosensors, and Figures S1−S3 (PDF)

AUTHOR INFORMATION

Corresponding Authors

Ruo Yuan − *Key Laboratory of Luminescence Analysis and Molecular Sensing (Southwest University), Ministry of Education, College of Chemistry and Chemical Engineering, Southwest University, Chongqing 400715, People's Republic of China;* orcid.org/0000-0003-3664-6236; Phone: +86-23-68252277; Email: yuanruo@swu.edu.cn; Fax: +86-23-68253172

Yaqin Chai − *Key Laboratory of Luminescence Analysis and Molecular Sensing (Southwest University), Ministry of Education, College of Chemistry and Chemical Engineering, Southwest University, Chongqing 400715, People's Republic of China;* orcid.org/0000-0003-4392-9592; Email: yqchai@swu.edu.cn

Authors

Ying Liu − *Key Laboratory of Luminescence Analysis and Molecular Sensing (Southwest University), Ministry of Education, College of Chemistry and Chemical Engineering, Southwest University, Chongqing 400715, People's Republic of China*

Lingqi Kong − *Key Laboratory of Luminescence Analysis and Molecular Sensing (Southwest University), Ministry of Education, College of Chemistry and Chemical Engineering, Southwest University, Chongqing 400715, People's Republic of China*

Hao Li − *Key Laboratory of Luminescence Analysis and Molecular Sensing (Southwest University), Ministry of Education, College of Chemistry and Chemical Engineering, Southwest University, Chongqing 400715, People's Republic of China*

Complete contact information is available at: https://pubs.acs.org/10.1021/acs.analchem.2c00613

Notes

The authors declare no competing financial interest.

ACKNOWLEDGMENTS

This work was financially supported by the NNSF of China (22176153, 22174113, and 21974108) and the Fundamental Research Funds for the Central Universities (XDJK2020TY002).

REFERENCES

(1) Tian, F.; Wang, S.; Shi, K.; Zhong, X.; Gu, Y.; Fan, Y.; Zhang, Y.; Yang, M. *Adv. Sci.* **2021**, *8*, 2102595.

(2) Nishizawa, M.; Walinda, E.; Morimoto, B.; Kohn, B.; Scheler, U.; Shirakawa, M.; Sugase, K. *J. Am. Chem. Soc.* **2021**, *143*, 11982−11993.

(3) Mishra, A.; Dhiman, S.; George, J. S. *Angew. Chem., Int. Ed.* **2021**, *60*, 2740−2756.

(4) Deng, J.; Walther, A. *Adv. Mater.* **2020**, *32*, 2002629.

(5) Ruan, Y. F.; Wang, H. Y.; Shi, X. M.; Xu, Y. T.; Yu, X. M.; Zhao, W. W.; Chen, H. Y.; Xu, J. J. Y. *Anal. Chem.* **2021**, *93*, 1200−1208.

(6) Ren, T. B.; Wen, S. Y.; Wang, L.; Lu, P.; Xiong, B.; Yuan, L.; Zhang, X. B. *Anal. Chem.* **2020**, *92*, 4681−4688.

(7) Zhang, Y.; Qi, G. H.; Wang, B.; Wang, D. D.; Jin, Y. D. *Anal. Chem.* **2020**, *92*, 3882−3887.

(8) Li, S.; Zhao, X. T.; Yu, X. X.; Wan, Y. Q.; Yin, M. Y.; Zhang, W. W.; Cao, B. Q.; Wang, H. *Anal. Chem.* **2019**, *91*, 14737−14742.

(9) Li, Z. L.; Li, S. K.; Guo, Y. H.; Yuan, C. Q.; Yan, X. H.; Schanze, K. S. *ACS Nano* **2021**, *15*, 4979−4988.

(10) Zhao, D.; Chang, D. G.; Zhang, Q.; Chang, Y. Y.; Liu, B.; Sun, C. S.; Li, Z. P.; Dong, C.; Liu, M.; Li, Y. F. *J. Am. Chem. Soc.* **2021**, *143*, 15084−15090.

(11) Chang, J. F.; Lv, W. X.; Li, Q.; Li, H. Y.; Li, F. *Anal. Chem.* **2020**, *92*, 8959−8964.

(12) Zhang, X. W.; Lazenby, R. A.; Wu, Y.; White, R. J. *Anal. Chem.* **2019**, *91*, 11467−11473.

(13) Kelly, L.; Maier, K. E.; Yan, A.; Levy, M. *Nat. Commun.* **2021**, *12*, 6275.

(14) Duan, Z. J.; Tan, L. X.; Duan, R. L.; Chen, M. G.; Xia, F.; Huang, F. J. *Anal. Chem.* **2021**, *93*, 11547−11556.

(15) He, H. F.; Dai, J. Y.; Dong, G. X.; Shi, H. L.; Wang, F.; Qiu, Y. R.; Liao, R. X.; Zhou, C. S.; Guo, Y.; Xiao, D. *Anal. Chem.* **2019**, *91*, 3043−3047.

(16) Lopez, A.; Liu, J. W. *Anal. Chem.* **2021**, *93*, 3018−3025.

(17) Chen, Z. M.; Wang, Y.; Du, X. Y.; Sun, J. J.; Yang, S. *Anal. Chem.* **2021**, *93*, 7843−7850.

(18) Li, H.; Kou, B. B.; Yuan, Y. L.; Chai, Y. Q.; Yuan, R. *Biosens. Bioelectron.* **2022**, *197*, 113758.

(19) Liang, Y. Y.; Wu, C. T.; Figueroa-Miranda, G.; Offenhäusser, A.; Mayer, D. *Biosens. Bioelectron.* **2019**, *144*, 111668.

(20) Wei, B. M.; Zhang, J. T.; Ou, X. W.; Lou, X. D.; Xia, F.; Vallée-Bélisle, A. *Anal. Chem.* **2018**, *90*, 1506−1510.

(21) Zheng, G. L.; Zhao, L.; Yuan, D. Y.; Li, J.; Yang, G.; Song, D. X.; Miao, H.; Shu, L. J.; Mo, X. M.; Xu, X. D.; Li, L.; Song, X.; Zhao, Y. Y. *Biosens. Bioelectron.* **2022**, *198*, 113827.

(22) Zhang, L. Q.; Wan, S.; Jiang, Y.; Wang, Y. Y.; Fu, T.; Liu, Q. L.; Cao, Z. J.; Qiu, L. P.; Tan, W. H. *J. Am. Chem. Soc.* **2017**, *139*, 2532−2540.

(23) Shi, X. B.; He, Y.; Gao, W. L.; Liu, X. Y.; Ye, Z. G.; Liu, H.; Xiao, L. H. *Anal. Chem.* **2018**, *90*, 3661−3665.

(24) Zhang, X. Y.; Song, C. X.; Yang, K.; Hong, W. W.; Lu, Y.; Yu, P.; Mao, L. Q. *Anal. Chem.* **2018**, *90*, 4968−4971.

(25) Fan, Y. Y.; Mou, Z. L.; Wang, M.; Li, J.; Zhang, J.; Dang, F. Q.; Zhang, Z. Q. *Anal. Chem.* **2018**, *90*, 13708−13713.

(26) He, H. F.; Dai, J. Y.; Dong, G. X.; Shi, H. L.; Wang, F.; Qiu, Y. R.; Liao, R. X.; Zhou, C. S.; Guo, Y.; Xiao, D. *Anal. Chem.* **2019**, *91*, 3043−3047.

(27) Chen, Z. M.; Mou, Q.; Wu, S. H.; Xie, Y.; Salminen, K.; Sun, J. J. *Anal. Chem.* **2022**, *94*, 1397−1405.
(28) Zhang, Y. T.; Figueroa-Miranda, G.; Wu, C. T.; Willbold, D.; Offenhäusser, A.; Mayer, D. *Nanoscale* **2020**, *12*, 16501−16513.
(29) Chen, C. X.; Zhao, D.; Jiang, Y. Y.; Ni, P. J.; Zhang, C. H.; Wang, B.; Yang, F.; Lu, Y. Z.; Sun, J. *Anal. Chem.* **2019**, *91*, 15017−15024.
(30) Chen, Q. S.; Zhang, Y. W.; Chen, H.; Liu, J. B.; Liu, J. W. *Anal. Chem.* **2021**, *93*, 8577−8584.
(31) Geng, X.; Sun, Y.; Guo, Y.; Zhao, Y.; Zhang, K.; Xiao, L.; Qu, L.; Li, Z. *Anal. Chem.* **2020**, *92*, 7940−7946.
(32) Li, L.; Lv, W. Y.; Wang, Y.; Li, Y. F.; Li, C. M.; Huang, C. Z. *Anal. Chem.* **2021**, *93*, 15331−15339.
(33) Chen, Z. M.; Wang, Y.; Du, X. Y.; Sun, J. J.; Yang, S. *Anal. Chem.* **2021**, *93*, 7843−7850.
(34) Zheng, J. Y.; Li, X. X.; Wang, K.; Song, J. J.; Qi, H. L. *Anal. Chem.* **2020**, *92*, 10940−10945.

Recommended by ACS

Enhanced Sensing Performance of a Microchannel-Based Electrochemiluminescence Biosensor for Adenosine Triphosphate via a dsDNA Superstructure Amplification...

Yanling Huang, Zhenyu Lin, *et al.*
AUGUST 02, 2022
ACS APPLIED MATERIALS & INTERFACES
READ

Molecular Recognition-Triggered Aptazyme Sensor Using a Co-MOF@MCA Hybrid Nanostructure as Signal Labels for Adenosine Triphosphate Detection in Food Samples

Ruina Zheng, Huali Jin, *et al.*
SEPTEMBER 07, 2022
ANALYTICAL CHEMISTRY
READ

Simultaneous Monitoring of the Adenosine Triphosphate Levels in the Cytoplasm and Nucleus of a Single Cell with a Single Nanowire-Based Fluorescent Biosensor

Mingliang Mei, Wensheng Shi, *et al.*
AUGUST 04, 2022
ANALYTICAL CHEMISTRY
READ

Versatile Electrochemiluminescence Biosensing Platform Based on DNA Nanostructures and Catalytic Hairpin Assembly Signal Amplification

Linying Yu, Xiurong Yang, *et al.*
AUGUST 04, 2022
ANALYTICAL CHEMISTRY
READ

Get More Suggestions >

https://doi.org/10.1021/acs.analchem.2c00613
Anal. Chem. 2022, 94, 6819−6826